SUPPLEMENTAL MATERIAL

Unveiling and Manipulating Hidden Symmetries in Graphene Nanoribbons

Nikita V. Tepliakov,[1,2,*] Johannes Lischner,[1,2] Efthimios Kaxiras,[3,4] Arash A. Mostofi,[1,2] and Michele Pizzochero[3,†]

[1] *Departments of Materials and Physics, Imperial College London, London SW7 2AZ, United Kingdom*
[2] *The Thomas Young Centre for Theory and Simulation of Materials, Imperial College London, London SW7 2AZ, United Kingdom*
[3] *School of Engineering and Applied Sciences, Harvard University, Cambridge, Massachusetts 02138, United States*
[4] *Department of Physics, Harvard University, Cambridge, Massachusetts 02138, United States*

(Dated: January 5, 2023)

CONTENTS

Supplemental Note 1:
Ab initio determination of hopping parameters in armchair graphene nanoribbons S1

Supplemental Note 2:
Nature of energy gaps in armchair graphene nanoribbons S2

Supplemental Note 3:
Robustness of the semimetallic state in graphene S2

Supplemental Note 4:
Analytical solutions of the tight-binding Hamiltonian S2

Supplemental Note 5:
Hidden four-fold rotational symmetry S4

Supplemental Note 6:
Localization effects in armchair graphene nanoribbons S4

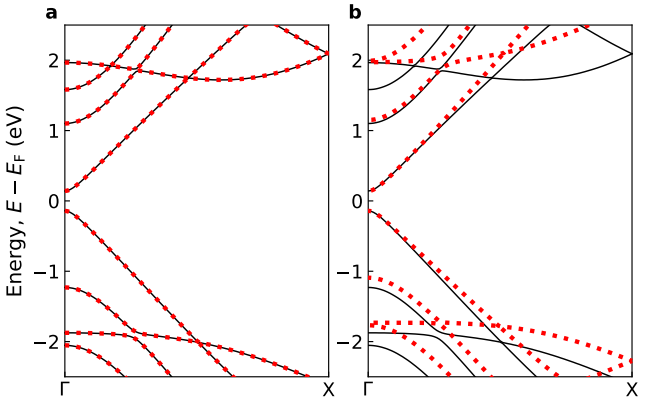

FIG. S1. Band structure of an armchair graphene nanoribbon of width $n = 8$. Black solid lines correspond to the first-principles calculations whereas the red dots are the energy bands originating from the p_z-orbitals, as obtained (a) through Wannierization of first-principles calculations and (b) tight-binding Hamiltonian with parameters t_1, t_2, t_3, and Δt_1 given in Supplemental Note 1.

SUPPLEMENTAL NOTE 1: *AB INITIO* DETERMINATION OF HOPPING PARAMETERS IN ARMCHAIR GRAPHENE NANORIBBONS

To accurately quantify the hopping interactions between p_z-orbitals in armchair graphene nanoribbons, we perform first-principles calculations in the density-functional theory formalism, as implemented in the Quantum ESPRESSO package [34, 35]. We rely on the generalized-gradient approximation of Perdew, Burke, and Ernzerhof [36]. We set the wavefunction (charge density) cutoff to 80 Ry (360 Ry), and sample the Brillouin zone with 12 and 24 k-points in the geometry optimization and band structure calculations, respectively. We introduce a vacuum region 15-Å thick in the non-periodic directions to avoid artificial interactions between periodic replicas.

The resulting first-principles calculations are subsequently used to construct projector Wannier functions of the p_z-orbitals of carbon atoms, taking advantage of the Wannier90 package [37]. In order to disentangle the energy bands arising from the p_z-orbitals, we consider the outer energy window, which contains *all* the bands originating from the p_z-orbitals, and the inner frozen window, in which the energy bands are contributed *only* by the p_z-orbitals. In Fig. S1(a), we compare the band structure of a representative armchair graphene nanoribbon obtained from first-principles and Wannier calculations.

Upon Wannierization, we find that the bulk values of hopping parameters in armchair graphene nanoribbons are $t_1 = -2.88$ eV, $t_2 = 0.22$ eV, and $t_3 = -0.25$ eV. Importantly, t_1 changes by $\Delta t_1 = -0.20$ eV at the edges of the nanoribbon due to the shortening of the carbon-carbon bond lengths. Fig. S1(b) shows the band structure of a representative armchair graphene nanoribbon obtained using the tight-binding Hamiltonian with these values of the hopping parameters, which is found to be in excellent agreement with the first-principles result at low energies.

In order to model the effect of lattice strain on the electronic structure of the nanoribbons, first we increase the

lattice constant by ε and optimize the atomic positions from first-principles calculations and then perform the same Wannierization procedure discussed above to extract the hopping parameters. The hopping parameters are found to vary with the lattice strain as

$$t_i(\varepsilon) = t_i(0)e^{-\gamma[a_i(\varepsilon)/a_i(0)-1]}, \tag{S1}$$

where $i = 1, 2, 3$ corresponds to the three distinct hopping interactions, $\gamma = 2.0$ is the spatial decay rate, and $a_i(\varepsilon)$ is the distance between i-th nearest neighbors in the nanoribbon under tensile strain. A similar relationship describes $\Delta t_1(\varepsilon)$.

SUPPLEMENTAL NOTE 2: NATURE OF ENERGY GAPS IN ARMCHAIR GRAPHENE NANORIBBONS

The inclusion of the third nearest-neighbor hopping interactions t_3 and the structural distortions at the edge of the nanoribbon (which results in a local increase of the first nearest-neighbor hopping interaction by Δt_1) in the tight-binding Hamiltonian is key to open the energy gap in armchair graphene nanoribbons of width $n = 3p + 2$. In order to quantify the relative importance of these two mechanisms in the energy-gap opening, we perform two distinct calculations:

1. We ignore the structural distortion at the edges, but account for hopping interactions up to t_3;

2. We ignore the third nearest-neighbor hopping interactions t_3, but account for the structural distortion at the edges through the corresponding local change in the hopping interaction Δt_1.

The result of these calculations reveal that both the structural distortion at the edges and the third-nearest neighbor hopping interactions are important to shape the energy gap of armchair graphene nanoribbons, with t_3 providing a slightly larger contribution by $\sim$20%.

SUPPLEMENTAL NOTE 3: ROBUSTNESS OF THE SEMIMETALLIC STATE IN GRAPHENE

Contrary to armchair graphene nanoribbons, the band structure of graphene remains semimetallic irrespective of the strength of long-range next-neighbor hopping interactions between the p_z-orbitals. The tight-binding Hamiltonian of graphene, written in the basis of two sublattices A and B, reads [38]

$$\hat{\mathcal{H}}_{\mathbf{k}} = \begin{pmatrix} h_2(\mathbf{k}) & h_1(\mathbf{k}) + h_3(\mathbf{k}) \\ h_1^\dagger(\mathbf{k}) + h_3^\dagger(\mathbf{k}) & h_2(\mathbf{k}) \end{pmatrix}, \tag{S2}$$

where

$$h_1(\mathbf{k}) = t_1 \left[e^{ik_y a} + 2\cos\frac{\sqrt{3}k_x a}{2} e^{-ik_y a/2} \right], \tag{S3}$$

$$h_2(\mathbf{k}) = 2t_2 \left[\cos(\sqrt{3}k_x a) + 2\cos\frac{\sqrt{3}k_x a}{2} \cos\frac{3k_y a}{2} \right], \tag{S4}$$

$$h_3(\mathbf{k}) = t_3 \left[e^{-2ik_y a} + 2\cos(\sqrt{3}k_x a) e^{ik_y a} \right], \tag{S5}$$

and a is the C-C bond length. Around the K point of the Brillouin zone, this Hamiltonian can be simplified as

$$\hat{\mathcal{H}}_{\mathbf{k}} = \begin{pmatrix} -3t_2 & (1 - 2t_3/t_1)v_{\mathrm{F}} q_+ \\ (1 - 2t_3/t_1)v_{\mathrm{F}} q_- & -3t_2 \end{pmatrix}, \tag{S6}$$

where $q_\pm = q_x \pm i q_y$, $\mathbf{q} = \mathbf{k} - \mathrm{K}$ is the electron momentum relative to the K point and $v_{\mathrm{F}} = 3t_1 a/2$ is the Fermi velocity. The diagonalization of this Hamiltonian yields

$$E_\pm(\mathbf{k}) = -3t_2 \pm \left(1 - \frac{2t_3}{t_1}\right) v_{\mathrm{F}} |\mathbf{q}|. \tag{S7}$$

Hence, the addition of second and third nearest-neighbor hopping interactions, t_2 and t_3, is ineffective in opening the energy gap in graphene, which remains semimetallic at $\mathbf{q} = 0$. Unlike armchair graphene nanoribbons, in graphene t_3 merely renormalizes the Fermi velocity as

$$\tilde{v}_{\mathrm{F}} = \left(1 - \frac{2t_3}{t_1}\right) v_{\mathrm{F}}. \tag{S8}$$

It is worth noticing in this context that an advantage of this low-energy approximation of the band structure of graphene is the possibility to adopt a scalable tight-binding model Hamiltonian for simulating properties of artificial honeycomb lattices, as proposed in Ref. [39]. According to this scalable tight-binding model, the bond length and the nearest-neighbor hopping parameter of pristine graphene are scaled as $a \to s_{\mathrm{f}} a$ and $t_1 \to t_1/s_{\mathrm{f}}$, where s_{f} is the scaling factor. Eq. (S7) implies that the scalable tight-binding approach can be further extended by including t_3, provided that such parameter is scaled analogously to t_1, that is, $t_3 \to t_3/s_{\mathrm{f}}$.

SUPPLEMENTAL NOTE 4: ANALYTICAL SOLUTIONS OF THE TIGHT-BINDING HAMILTONIAN

At the nearest-neighbor tight-binding level, the Hamiltonian of the auxiliary model shown in Fig. 1(a) can be solved analytically. First, we note that the square lattice is separable in Cartesian coordinates x and y, i.e.,

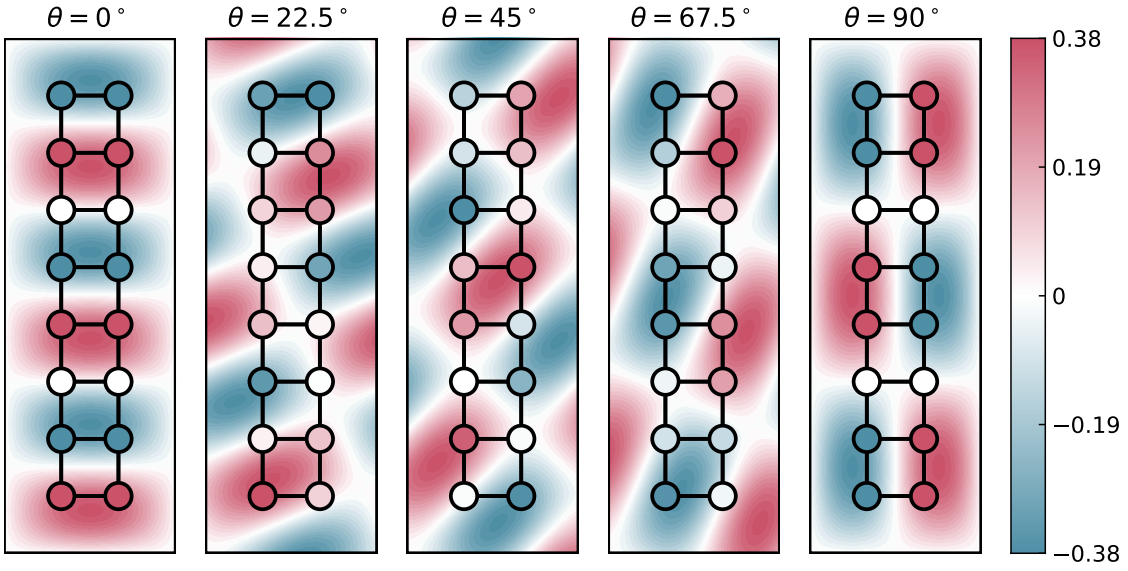

FIG. S2. Rotation of the degenerate state with indices $(1, 2p+2) = (1, 6)$ in the quantum box corresponding to the auxiliary model with $n = 8$ by an angle θ. Upon four-fold rotation ($\theta = 90°$), this state transforms into the other degenerate state $(2, p+1) = (2, 3)$, up to a minus sign.

it can be decoupled in two perpendicular sets of one-dimensional chains. A one-dimensional chain of infinite length has a straightforward solution of the form

$$\psi_k(\xi_i) = Ae^{ik\xi_i} + Be^{-ik\xi_i}, \tag{S9a}$$

$$E_k = 2t_1 \cos k, \tag{S9b}$$

where we set the lattice constant to unity, t_1 is the nearest-neighbor hopping amplitude, and ξ_i is the coordinate of the i-th lattice site. In a finite chain comprising n sites located at $\xi_i = 1, 2, \ldots, n$, the wavefunction must vanish outside the chain region. This is described by the boundary condition

$$\psi_k(0) = \psi_k(n+1) = 0, \tag{S10}$$

which enforces the quantization of the electron momentum as

$$k = \frac{\pi m}{n+1}, \tag{S11}$$

where $m = 1, 2, \ldots, n$ labels the energy states of the chain. The normalized wavefunctions and the energies are then given by

$$\psi_m(\xi_i) = \sqrt{\frac{2}{n+1}} \sin\left(\frac{\pi m \xi_i}{n+1}\right), \tag{S12a}$$

$$E_m = 2t_1 \cos\left(\frac{\pi m}{n+1}\right). \tag{S12b}$$

The wavefunctions of the chain of n sites are identical to continuum wavefunctions of an infinite quantum well of width $(n+1)$, albeit with different energies.

This analytical result is easily generalized to the case of the auxiliary model which is a lattice of $2 \times n$ sites (i.e., the two-leg ladder lattice), yielding

$$E_{m_x m_y} = 2t_1 \left[\cos\left(\frac{\pi m_x}{3}\right) + \cos\left(\frac{\pi m_y}{n+1}\right)\right], \tag{S13a}$$

$$\psi_{m_x m_y}(x_i, y_i) = \frac{2}{\sqrt{3(n+1)}} \sin\left(\frac{\pi m_x x_i}{3}\right) \sin\left(\frac{\pi m_y y_i}{n+1}\right), \tag{S13b}$$

where x_i and y_i are the Cartesian coordinates of the i-th site of the auxiliary model. Since the n-site chain is equivalent to an infinite well of size $(n+1)$, then the auxiliary model of size $2 \times n$ is equivalent by analogy to a two-dimensional quantum box of dimensions $3 \times (n+1)$, where the quantum numbers labeling the states take values $m_x = 1, 2$ and $m_y = 1, 2, \ldots, n$, so that in total there are $2n$ states.

The wavefunctions $\psi_{m_x m_y}(x_i, y_i)$ are discrete and provide the coefficients of the eigenvectors on the i-th site with Cartesian coordinates x_i and y_i. This wavefunction can be viewed as the mapping of the continuous wavefunction $\psi_{m_x m_y}(x, y)$, which spans over the entire two-dimensional space, onto the lattice sites of the auxiliary model. This is why the hidden symmetry operator acting on these states can transform them into the other eigenstates of the auxiliary model despite the lack of a spatial four-fold rotational symmetry $\hat{C}_4$.

SUPPLEMENTAL NOTE 5: HIDDEN FOUR-FOLD ROTATIONAL SYMMETRY

The auxiliary model has a hidden symmetry associated with the four-fold rotation $\hat{C}_4$ around one of its corners, analogously to the simple model of the rectangular quantum box presented in Supplemental Note 4. The degenerate modes of the auxiliary model $|\psi\rangle$ and $|\phi\rangle$, which correspond to the states $(1,2p+2)$ and $(2,p+1)$ in the quantum box, are connected through the hidden symmetry as $|\psi\rangle = -\hat{C}_4|\phi\rangle$ [40]. In Fig. S2, we depict the four-fold rotation of such states.

SUPPLEMENTAL NOTE 6: LOCALIZATION EFFECTS IN ARMCHAIR GRAPHENE NANORIBBONS

At the nearest-neighbor tight-binding level, armchair graphene nanoribbons of width $n = 3p+2$ exhibit a pair of zero-energy states at the Γ point of the Brillouin zone. In the corresponding auxiliary model, the wavefunctions of the zero-energy states localize in a distinct pattern that consists of regions of square symmetry. In Fig. S3, we expand our investigation by inspecting the wavefunctions of all the sixteen energy levels of the auxiliary model for the representative case $n = 8$, and of cyclobutadiene (C_4H_4) for comparison. Remarkably, we note that, in addition to the pair of zero-energy states denoted $|8\rangle$ and $|9\rangle$, there are two additional states $|3\rangle$ and $|14\rangle$ which are localized in a similar square-shaped pattern. Within each square region, these states are reminiscent of the non-degenerate ground and second excited states of cyclobutadiene, in the same way that $|8\rangle$ and $|9\rangle$ resemble its zero-energy modes. These four states are observed in all armchair graphene nanoribbons of the $n = 3p+2$ family.

* n.tepliakov20@imperial.ac.uk
† mpizzochero@g.harvard.edu

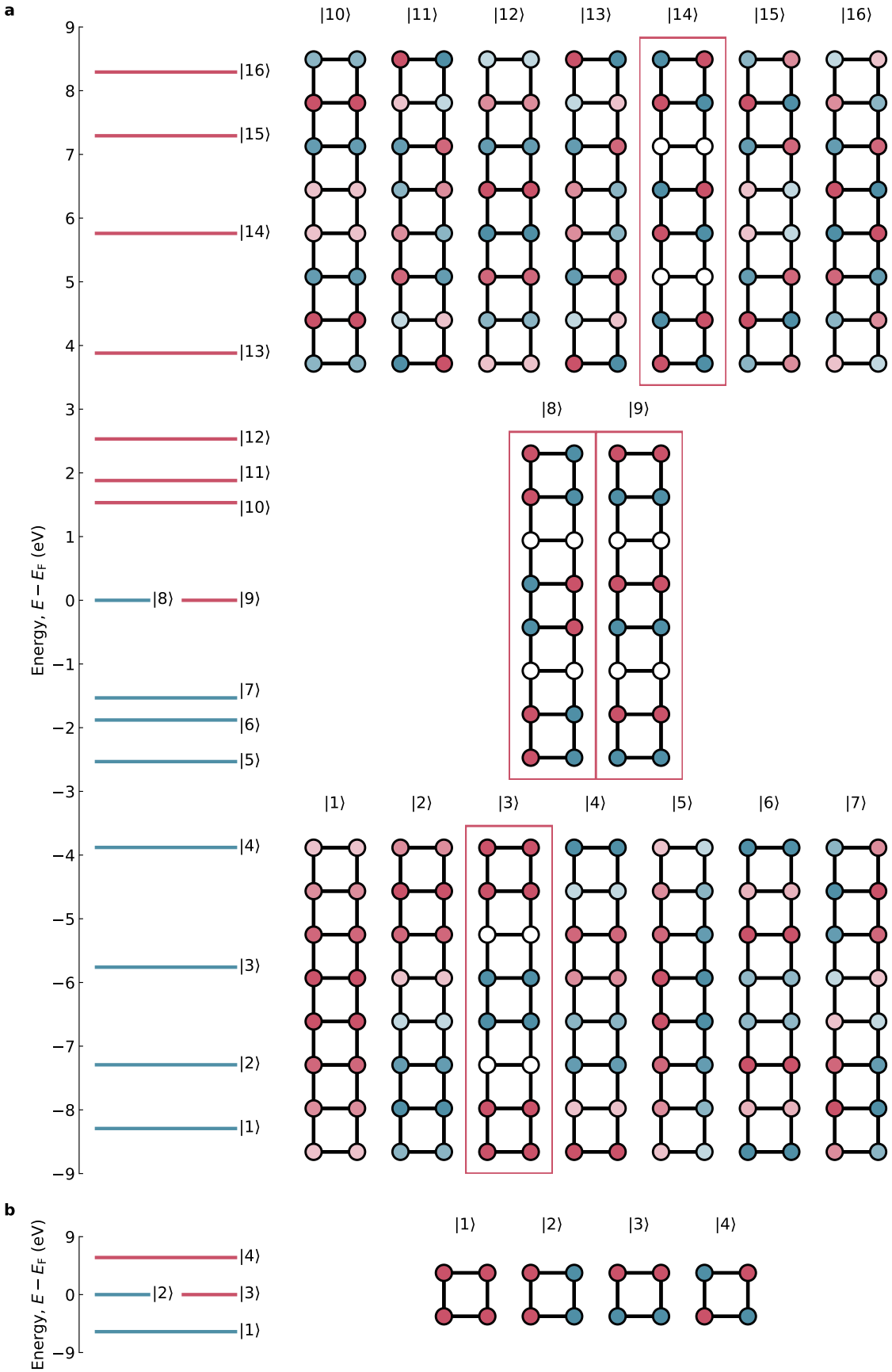

FIG. S3. Energy spectrum and corresponding wavefunctions of (a) the auxiliary model for the representative case $n = 8$ and (b) cyclobutadiene, as obtained at the nearest-neighbor tight-binding level.